



Cite this: DOI: 10.1039/d1dt01621k

Received 19th May 2021

Accepted 20th July 2021

DOI: 10.1039/d1dt01621k

rsc.li/dalton

Precise incorporation of transition metals into organolead oxyhalide crystalline materials for photocatalysis†

Lu Zhang,[‡] Wen Ma,[‡] Chen Sun, Lei Fang, Xueling Song and Honghan Fei *

Organolead halide crystalline materials are an emerging class of high-performance photocatalysts. However, limited studies have been performed to tune their photoactive properties by precise introduction of transition metals. Herein, we report the successful incorporation of four different transition metal centers (Mn^{2+} , Co^{2+} , Ni^{2+} and Zn^{2+}) into a lead oxyhalide crystalline matrix *via* isoreticular synthesis. Importantly, the precise control of the incoming transition metal positions has been achieved by its octahedral coordination with three organic ligands. Among them, the Zn^{2+} -incorporated material exhibits the highest catalytic activity and recyclable activity in benzylamine oxidation under UV light, which is probably ascribed to the long carrier lifetime and efficient carrier transfer.

The family of inorganic–organic hybrid lead halide materials is an intriguing class of photoactive materials with tunable bandgaps and excellent carrier transport characteristics for photovoltaic cells and light-emitting diodes.^{1–4} In recent years, their advantageous photochemical properties have made them an emerging class of semiconducting photocatalysts.^{5–8} For example, Nam and co-workers reported the photocatalytic splitting of hydriodic acid to produce hydrogen using methylammonium lead iodide (MAPbI₃) with an overall efficiency of 0.81%, of which the high concentrations of H⁺ and I[−] are critical to dynamically stabilize the tetragonal MAPbI₃ phase.⁹ Subsequently, enhanced photocatalytic performances of MAPbI₃ in hydrogen evolution in HI solution have been achieved by forming composites with reduced graphene oxide,¹⁰ TiO₂¹¹ and Ni₃C.¹² However, the moisture-sensitive nature remains to be a bottleneck issue. Very recently, our

group developed a chemically stable organolead iodide material by crystal engineering using anionic organic ligands. The reported [Pb₈I₈(H₂O)₃]⁸⁺([−]O₂C(CH₂)₄CO₂[−])₄ material has suitable band positions and long carrier lifetimes, leading to high efficiency for overall photocatalytic water splitting.¹³

Incorporation of a new metal cation or anion, such as doping, ion insertion and/or forming a solid solution, is a powerful synthetic strategy to tune the bandgaps and/or carrier properties of inorganic semiconductors, which may substantially improve their photocatalytic properties.¹⁴ Tuning the anion composition is more commonly observed in organolead halide perovskites, owing to the predominantly halide-based valence bands.^{15,16} Importantly, the synergy effects of bi-metallic materials have been successfully applied for designing photocatalysts, because the fine control and design of the molecular structure are capable of creating metal-to-metal charge transfer (MMCT) or appropriate oxidation/reduction potential, leading to excellent photoelectric properties.^{17–19} Recently, transition metals have been successfully introduced into the lattice, providing another synthetic tool to control the optoelectronic properties of lead halide perovskites.^{14,20,21} The incorporation of Zn²⁺ cations is found to increase the bandgap of CsPbBr₃ nanocrystals owing to lattice contraction.²² Meanwhile, the doping of Mn²⁺ facilitates the energy transfer between the metal halide hosts and the dopants.²³ In addition, Zn²⁺ dopants in Ga₂O₃ will introduce new mid-gap states, which serve as electron traps, limit electron–hole recombination and increase the photocarrier lifetime.²⁴ Moreover, precise atomic control of the incoming metal centers will be highly desired to elucidate their influences on the semiconductive metal halide host and may further tailor and/or enhance the photocatalytic performances.²⁵ However, it remains a great challenge to incorporate new metal centers into the metal halide in an atomically precise manner, which has been studied in metal chalcogenides.^{26,27}

Herein, we report the isoreticular synthesis of bimetallic organometal oxohalide frameworks, which consist of 3-D cationic [Pb₈O(OH)Br₉]⁴⁺ frameworks with the insertion of tran-

Shanghai Key Laboratory of Chemical Assessment and Sustainability, School of Chemical Science and Engineering, Tongji University, 1239 Siping Rd., Shanghai 200092, P. R. China. E-mail: fei@tongji.edu.cn

† Electronic supplementary information (ESI) available: Experimental details and additional characterization. CCDC 2082662. For ESI and crystallographic data in CIF or other electronic format see DOI: 10.1039/d1dt01621k

‡ These authors contributed equally.

sition metal-based $[\text{ML}_3]^{4-}$ clusters (M: divalent transition metals; L: $^-\text{O}(\text{CH}_2)_2\text{O}^-$). Intriguingly, the atomically-precise transition metal sites could be occupied by four different metal centers, including Mn^{2+} , Co^{2+} , Ni^{2+} and Zn^{2+} . Among the four materials, the Zn^{2+} -incorporated organolead oxohalide material exhibits enhanced photocatalytic benzylamine oxidation performance, ascribed to its longer photocarrier lifetime and better photocarrier transport property.

The solvothermal reaction of $\text{Pb}(\text{NO}_3)_2$, KBr and $\text{Mn}(\text{OAc})_2$ in ethylene glycol afforded yellow block-shaped crystals of $[\text{Pb}_8\text{O}(\text{OH})\text{Br}_9][\text{MnL}_3]$ (L^{2-} : $^-\text{O}(\text{CH}_2)_2\text{O}^-$), which we denote as TJU-18(Pb/Mn) (TJU = Tongji University). Ethylene glycol was employed as both the organic ligand and the synthetic solvent. X-ray crystallography revealed that TJU-18(Pb/Mn) consists of cationic $[\text{Pb}_8\text{O}(\text{OH})\text{Br}_8]^{4+}$ layered networks with discrete Br^- anions and $[\text{MnL}_3]^{4-}$ clusters residing in the interlamellar region (Fig. 1a). In each $[\text{Pb}_8\text{O}(\text{OH})\text{Br}_8]^{4+}$ layer, the inorganic connectivity propagates along the *c*-axis to form chains that are connected by Pb–Br bonding (Fig. 1b and S1, ESI†). All of the intralayer Br and O in the structure are μ_3 -bridging towards Pb^{2+} centers, which are important to their stability in polar organic solvents (discussed later). The adjacent layers are linked by interlamellar μ_2 -Br with a Pb–Br–Pb bond angle of $125.19(1)^\circ$. The large interlayer spacing allows for the insertion of $[\text{MnL}_3]^{4-}$ clusters. All of the three ethylene glycol ligands in each cluster are fully deprotonated and bidentate towards Mn^{2+} centers, which occupy a distorted octahedral coordination. In addition, the oxygen atoms in the $[\text{MnL}_3]^{4-}$ clusters covalently interacted with the inorganic layers by forming Pb–O connectivity.

Importantly, the atomically-precise incorporation of transition metal centers was achieved by isorecticular synthesis but replacing the Mn^{2+} precursor with other first-row transition metal acetate (*e.g.* $\text{Co}(\text{OAc})_2$, $\text{Ni}(\text{OAc})_2$ and $\text{Zn}(\text{OAc})_2$), affording TJU-18(Pb/Co), TJU-18(Pb/Ni) and TJU-18(Pb/Zn), respectively. Single-crystal X-ray crystallography showed the isostructural nature in the $P2_1/n$ space group with only slight differences in unit cell volumes (0.19%) between TJU-18(Pb/Co) and TJU-18(Pb/Mn). PXRD of the as-synthesized materials confirmed that all of the four TJU-18 give the identical phase and match the

theoretical PXRD patterns based on the single-crystal solution of TJU-18(Pb/Mn) and TJU-18(Pb/Co) (Fig. 2a).

The four TJU-18 compounds are thermally stable up to 280°C , followed by decomposition of ethylene glycol, evidenced by thermogravimetric analysis (Fig. S2, ESI†). The chemical stability was determined by incubating (without magnetic stirring) the as-synthesized single crystals in polar organic solvents (EtOH, CH_3CN , DMF and DMA) at room temperature for 24 h. The high crystallinity and phase purity were well retained after these chemical treatments, evidenced by PXRD and a negligible decrease in the mass balance (Fig. S3, ESI†).

Ultraviolet–visible (UV–Vis) absorption spectroscopy demonstrates that the four TJU-18 materials have analogous bandgap energies (E_g) of 3.27 eV for TJU-18(Pb/Mn), 3.25 eV for TJU-18(Pb/Co), 3.23 eV for TJU-18(Pb/Ni) and 3.24 eV for TJU-18(Pb/Zn), respectively, according to the Kubelka–Munk

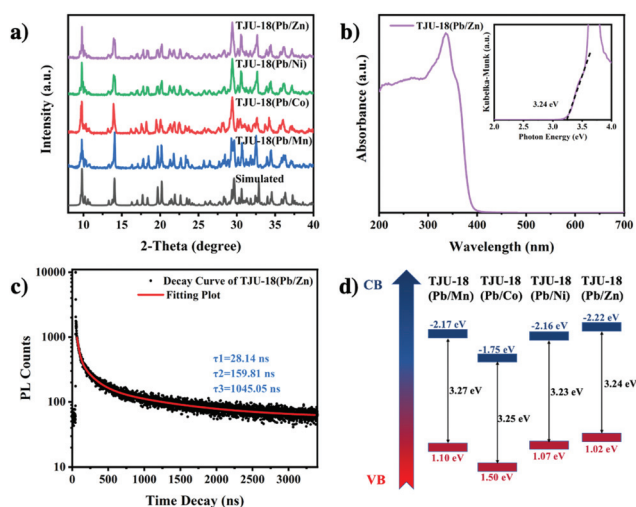


Fig. 2 (a) Powder XRD patterns of TJU-18(Pb/Mn), TJU-18(Pb/Co), TJU-18(Pb/Ni) and TJU-18(Pb/Zn). (b) UV–Vis absorption spectra and estimated bandgap energies of TJU-18(Pb/Zn). (c) Time-resolved transient PL decay of TJU-18(Pb/Zn). (d) Band energy diagram of TJU-18(Pb/Mn), TJU-18(Pb/Co), TJU-18(Pb/Ni) and TJU-18(Pb/Zn).

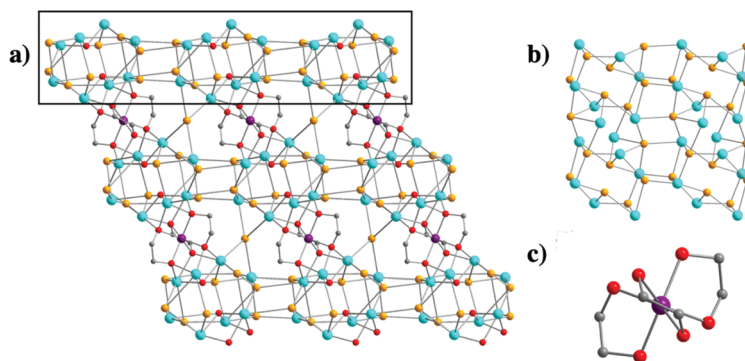


Fig. 1 (a) Crystallographic view of TJU-18(Pb/Mn) along the *b*-axis. (b) Crystallographic top-view of a single $[\text{Pb}_8\text{Br}_8\text{O}(\text{OH})]^{5+}$ layer along the *c*-axis. (c) Crystallographic view of a discrete $[\text{MnL}_3]^{4-}$ cluster (manganese: purple, lead: light blue, bromine: orange; oxygen: red; carbon: gray).

method (Fig. 2b and S4–S6, ESI†). The valence band levels of TJU-18 were determined from linear extrapolation of the valence-band-edge spectra measured by X-ray photoelectron spectroscopy (XPS),^{28,29} providing valence band values (vs. normal hydrogen electrode) of 1.10 eV for TJU-18(Pb/Mn), 1.50 eV for TJU-18(Pb/Co), 1.07 eV for TJU-18(Pb/Ni) and 1.02 eV for TJU-18(Pb/Zn), respectively (Fig. 2d and S7, ESI†). Furthermore, the DFT calculation demonstrated that the calculated bandgaps are 2.99 eV for TJU-18(Pb/Mn) and 2.81 eV for TJU-18(Pb/Zn), both of which are close to the experimental values. The Zn 4s and 3d orbitals of TJU-18(Pb/Zn) have negligible contributions to the top of the valence band (VB) and the bottom of the conduction band (CB), respectively (Fig. S8, ESI†). However, the Mn 4s orbitals of the control material TJU-18(Pb/Mn) have substantially larger contributions to both edges of the VB and CB (Fig. S9, ESI†), which probably enhances the radiative recombination of carriers and lowers the carrier lifetimes. Since the Pb orbitals also contribute to both VBM and CBM that may be detrimental to the charge separation,^{30,31} we have performed the calculations of the effective mass of charge carriers (Table S2†). For TJU-18(Pb/Zn), the effective mass of charge carriers is isotropic ($m_{G\rightarrow Z}^*/m_{G\rightarrow B}^* \approx 1.0$) and smaller, compared with that of TJU-18(Pb/Mn). These values indicate that TJU-18(Pb/Zn) has higher carrier transport effectiveness and better separation of electron–hole pairs.^{32,33}

Given the atomically precise incorporation of transition metal centers into our semiconductive metal oxybromide frameworks, we sought to investigate their influence on photocatalytic properties. Photocatalytic oxidation of primary amines is found to be an effective strategy to selectively afford imines, since the conventional synthesis of imines suffers from low selectivity and efficiency.^{34,35} Photocatalytic oxidation of benzylamine was performed in the presence of 3.8 mol% of the TJU-18 photocatalyst under 1 atm of O₂ in CH₃CN upon UV light illumination. It should be noted that TJU-18(Pb/Zn) showed a substantially higher photocatalytic yield (90%) than the other three TJU-18 materials (55–66%) (Table 1 entries 1–4). Control experiments without the photocatalyst or without light illumination were performed under identical conditions (Table 1, entries 5 and 6). Both reactions showed negligible conversion, demonstrating the important role of TJU-18 in the photocatalytic process. The use of other solvents (*e.g.* toluene, THF and acetone) significantly suppressed the turnover (Table 1, entries 7–9), which has been previously observed as well in other photocatalytic systems.^{36–38} Moreover, the control reaction catalyzed by Pb(NO₃)₂, Zn(OAc)₂, ZnO, and ZnBr₂ afforded substantially lower yields of the target products (Table 1, entries 10–13). Importantly, all of the four TJU-18 photocatalysts exhibited excellent recyclability without an obvious decrease in the yields over five photocatalytic cycles (Fig. 3a). Between each run, the catalysts could be recovered by filtration, washed with CH₃CN, and then directly used for additional cycles. The crystallinity of the organometal halide materials was maintained after five cycles, confirmed by the PXRD patterns (Fig. 3b).

Table 1 Oxidative coupling of benzylamines under various conditions

Entry	Catalyst	Solvents	$h\nu$	Yield (%)
1	TJU-18(Pb/Zn)	CH ₃ CN	+	90
2	TJU-18(Pb/Mn)	CH ₃ CN	+	66
3	TJU-18(Pb/Co)	CH ₃ CN	+	55
4	TJU-18(Pb/Ni)	CH ₃ CN	+	60
5	Blank	CH ₃ CN	+	10
6	TJU-18(Pb/Zn)	CH ₃ CN	–	10
7	TJU-18(Pb/Zn)	Toluene	+	<2
8	TJU-18(Pb/Zn)	Acetone	+	2
9	TJU-18(Pb/Zn)	THF	+	10
10	Pb(NO ₃) ₂	CH ₃ CN	+	19
11	Zn(OAc) ₂	CH ₃ CN	+	17
12	ZnO	CH ₃ CN	+	28
13	ZnBr ₂	CH ₃ CN	+	22

Reaction conditions: 0.1 mmol benzylamine, 10 mg catalyst, 300 W Hg lamp, 10 ml CH₃CN, 1 atm O₂, 6 h. ‘+’: under a 300 W Hg lamp, ‘–’: in darkness. Yields determined by ¹H NMR.

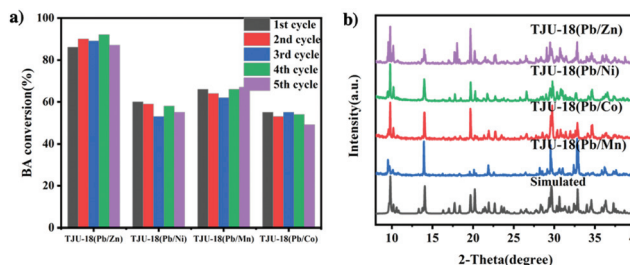


Fig. 3 (a) Recycling performance of TJU-18(Pb/Mn), TJU-18(Pb/Co), TJU-18(Pb/Ni) and TJU-18(Pb/Zn) toward oxidative coupling of benzylamines in different cycles. (b) XRD spectra after the photocatalysis of benzylamines for 5 cycles.

We performed additional photophysical experiments to further investigate why the incorporation of Zn²⁺ has a positive effect on photocatalysis. First, the band alignment of all four TJU-18 materials meets the requirement for the reduction of O₂ to a superoxide (O₂^{•−}) radical intermediate (−0.33 V vs. NHE), which enables them to be potentially active for photocatalytic oxidation (Fig. 2d). However, the PL decay curves at room temperature indicate that TJU-18(Pb/Zn) has an average PL lifetime of 220 ns, which is higher than the PL lifetimes of the other three materials (173 ns for TJU-18(Pb/Mn), 124 ns for TJU-18(Pb/Co) and 129 ns for TJU-18(Pb/Ni)) (Fig. S10–S12, ESI†). The higher photogenerated carrier lifetime of TJU-18 (Pb/Zn) probably limits the electron–hole recombination, improving their photocatalytic performance. Moreover, the transient photocurrent responses of TJU-18(Pb/Zn) in the photoelectrochemical tests were substantially higher than those of other TJU-18 materials under AM 1.5G simulated sunlight irradiation (Fig. 4b). The above-mentioned results demonstrate that the Zn²⁺ ion with a d¹⁰ electron configuration contributes to the enhanced transport property of the photo-

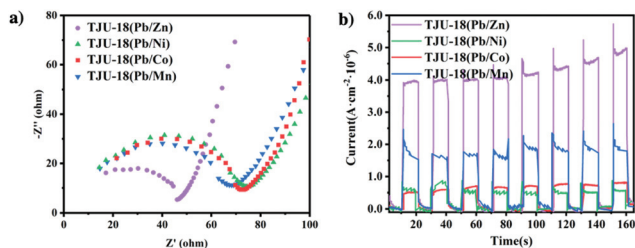


Fig. 4 (a) Nyquist plots measured at 0 V versus the Ag/AgCl electrode under light irradiation in the same solution with ECL measurement. (b) ECL transient spectra with step voltage measured in solution containing 0.1 M Na₂SO₄ as the electrolyte solution.

generated carriers in TJU-18(Pb/Zn). This is further supported by a smaller Nyquist plot diameter for TJU-18(Pb/Zn) than those of the other three materials, measured by electrochemical impedance spectroscopy (Fig. 4a). Overall, the improved photocatalytic performance of TJU-18(Pb/Zn) is largely ascribed to the enhanced separation of the photogenerated electron-hole pairs and the enhanced photocarrier transfer.

In conclusion, we successfully realized the atomically precise control of introducing four different transition metal centers (*i.e.* Mn²⁺, Co²⁺, Ni²⁺ and Zn²⁺) into an organolead oxybromide crystalline framework, which are structurally elucidated by X-ray crystallography. All of these semiconductive materials are chemically stable in a variety of organic solvents. Meanwhile, the photocatalytic properties of Zn²⁺-incorporated bimetallic oxyhalide are superior to those of other bimetallic members, probably owing to its enhanced carrier transport mobility. We are further extending this synthetic strategy to other lead halide materials, opening up an opportunity to finely tune their photoactive properties by atomically precise incorporation of transition metal centers.

Conflicts of interest

There are no conflicts to declare.

Acknowledgements

This work was supported by grants from the National Natural Science Foundation of China (21971197 and 51772217), the Shanghai Rising-Star Program (No. 20QA1409500), the Recruitment of Global Youth Experts by China and the Science & Technology Commission of Shanghai Municipality (19DZ2271500).

Notes and references

1 Q. Dong, Y. Fang, Y. Shao, P. Mulligan, J. Qiu, L. Cao and J. Huang, *Science*, 2015, **347**, 967–970.

- 2 G. Xing, N. Mathews, S. Sun, S. S. Lim, Y. M. Lam, M. Graetzel, S. Mhaisalkar and T. C. Sum, *Science*, 2013, **342**, 344–347.
- 3 Y. Yang, M. Yang, D. T. Moore, Y. Yan, E. M. Miller, K. Zhu and M. C. Beard, *Nat. Energy*, 2017, **2**, 16207.
- 4 J. Zhang, S. Ji, Y. Ma, R. Guan, X. Wu, X. Qu, B. Yan, D. Zhang, J. Zhao and J. Yang, *Nanoscale*, 2019, **11**, 11660–11670.
- 5 M. Que, Y. Zhao, L. Pan, Y. Yang, Z. He, H. Yuan, J. Chen and G. Zhu, *Mater. Lett.*, 2021, **282**, 128695.
- 6 Y.-C. Pu, H.-C. Fan, T.-W. Liu and J.-W. Chen, *J. Mater. Chem. A*, 2017, **5**, 25438–25449.
- 7 X. L. Zhu, Y. X. Lin, J. S. Martin, Y. Sun, D. Zhu and Y. Yan, *Nat. Commun.*, 2019, **10**, 10.
- 8 X. L. Zhu, Y. X. Lin, Y. Sun, M. C. Beard and Y. Yan, *J. Am. Chem. Soc.*, 2019, **141**, 733–738.
- 9 S. Park, W. J. Chang, C. W. Lee, S. Park, H.-Y. Ahn and K. T. Nam, *Nat. Energy*, 2016, **2**, 16185.
- 10 Y. Q. Wu, P. Wang, X. L. Zhu, Q. Q. Zhang, Z. Y. Wang, Y. Y. Liu, G. Z. Zou, Y. Dai, M. H. Whangbo and B. B. Huang, *Adv. Mater.*, 2018, **30**, 6.
- 11 X. M. Wang, H. Wang, H. F. Zhang, W. Yu, X. L. Wang, Y. Zhao, X. Zong and C. Li, *ACS Energy Lett.*, 2018, **3**, 1159–1164.
- 12 Z. J. Zhao, J. J. Wu, Y. Z. Zheng, N. Li, X. T. Li and X. Tao, *ACS Catal.*, 2019, **9**, 8144–8152.
- 13 X. Song, G. Wei, J. Sun, C. Peng, J. Yin, X. Zhang, Y. Jiang and H. Fei, *Nat. Catal.*, 2020, **3**, 1027–1033.
- 14 Y. Zhou, J. Chen, O. M. Bakr and H.-T. Sun, *Chem. Mater.*, 2018, **30**, 6589–6613.
- 15 M. M. Lee, J. Teuscher, T. Miyasaka, T. N. Murakami and H. J. Snaith, *Science*, 2012, **338**, 643–647.
- 16 M. Yang, T. Zhang, P. Schulz, Z. Li, G. Li, D. H. Kim, N. Guo, J. J. Berry, K. Zhu and Y. Zhao, *Nat. Commun.*, 2016, **7**, 12305.
- 17 R. Nakamura, A. Okamoto, H. Osawa, H. Irie and K. Hashimoto, *J. Am. Chem. Soc.*, 2007, **129**, 9596–9597.
- 18 M. Kaur, S. Pramanik, M. Kumar and V. Bhalla, *ACS Catal.*, 2017, **7**, 2007–2021.
- 19 H. Sakamoto, J. Imai, Y. Shiraishi, S. Tanaka, S. Ichikawa and T. Hirai, *ACS Catal.*, 2017, **7**, 5194–5201.
- 20 Q. A. Akkerman, D. Meggiolaro, Z. Dang, F. De Angelis and L. Manna, *ACS Energy Lett.*, 2017, **2**, 2183–2186.
- 21 J. Zhang, L. Zhang, P. Cai, X. Xue, M. Wang, J. Zhang and G. Tu, *Nano Energy*, 2019, **62**, 434–441.
- 22 W. van der Stam, J. J. Geuchies, T. Altantzis, K. H. W. van den Bos, J. D. Meeldijk, S. Van Aert, S. Bals, D. Vanmaekelbergh and C. de Mello Donega, *J. Am. Chem. Soc.*, 2017, **139**, 4087–4097.
- 23 W. Liu, Q. Lin, H. Li, K. Wu, I. Robel, J. M. Pietryga and V. I. Klimov, *J. Am. Chem. Soc.*, 2016, **138**, 14954–14961.
- 24 A. Yamakata, J. J. M. Vequizo, T. Ogawa, K. Kato, S. Tsuboi, N. Furutani, M. Ohtsuka, S. Muto, A. Kuwabara and Y. Sakata, *ACS Catal.*, 2021, **11**, 1911–1919.

- 25 E. C. Tyo and S. Vajda, *Nat. Nanotechnol.*, 2015, **10**, 577–588.
- 26 J. Lin, Y. Dong, Q. Zhang, D. Hu, N. Li, L. Wang, Y. Liu and T. Wu, *Angew. Chem., Int. Ed.*, 2015, **54**, 5103–5107.
- 27 J. Lin, Q. Zhang, L. Wang, X. Liu, W. Yan, T. Wu, X. Bu and P. Feng, *J. Am. Chem. Soc.*, 2014, **136**, 4769–4779.
- 28 X. Chen, L. Liu, P. Y. Yu and S. S. Mao, *Science*, 2011, **331**, 746–750.
- 29 L. Pan, J. H. Kim, M. T. Mayer, M.-K. Son, A. Ummadisingu, J. S. Lee, A. Hagfeldt, J. Luo and M. Grätzel, *Nat. Catal.*, 2018, **1**, 412–420.
- 30 Z. Xiao, Z. Song and Y. Yan, *Adv. Mater.*, 2019, **31**, 1803792.
- 31 W. Yin, T. Shi and Y. Yan, *Adv. Mater.*, 2014, **26**, 4653–4658.
- 32 H. Suzuki, S. Kanno, M. Hada, R. Abe and A. Saeki, *Chem. Mater.*, 2020, **32**, 4166–4173.
- 33 J. Even, L. Pedesseau, J.-M. Jancu and C. Katan, *J. Phys. Chem. Lett.*, 2013, **4**, 2999–3005.
- 34 M. Llargeron and M.-B. Fleury, *Science*, 2013, **339**, 43–44.
- 35 M. T. Schümperli, C. Hammond and I. Hermans, *ACS Catal.*, 2012, **2**, 1108–1117.
- 36 D. Sun, L. Ye and Z. Li, *Appl. Catal., B*, 2015, **164**, 428–432.
- 37 R. Liu, S. Meng, Y. Ma, L. Niu, S. He, X. Xu, B. Su, D. Lu, Z. Yang and Z. Lei, *Catal. Commun.*, 2019, **124**, 108–112.
- 38 S. Fountoulaki, P. L. Gkizis, T. S. Symeonidis, E. Kaminioti, A. Karina, I. Tamiolakis, G. S. Armatas and I. N. Lykakis, *Adv. Synth. Catal.*, 2016, **358**, 1500–1508.